AGU Advances

RESEARCH ARTICLE
10.1029/2022AV000849

Peer Review The peer review history for this article is available as a PDF in the Supporting Information.

Key Points:

- Ocean currents on icy moons such as Europa may drive rotation of their overlying ice shells
- A mathematical model for ice shell movements driven by ocean stress, shell elasticity and viscous adjustment is developed
- The model shows rotation rates slightly slower than synchronous and is used to constrain ice shell parameters such as effective viscosity

Supporting Information:

Supporting Information may be found in the online version of this article.

Correspondence to:

Y. Ashkenazy,
ashkena@bgu.ac.il

Citation:

Ashkenazy, Y., Tziperman, E., & Nimmo, F. (2023). Non-synchronous rotation on Europa driven by ocean currents. *AGU Advances*, *4*, e2022AV000849. https://doi.org/10.1029/2022AV000849

Received 17 NOV 2022
Accepted 23 MAR 2023

Author Contributions:

Conceptualization: Yosef Ashkenazy, Eli Tziperman, Francis Nimmo
Funding acquisition: Yosef Ashkenazy, Eli Tziperman, Francis Nimmo

Non-Synchronous Rotation on Europa Driven by Ocean Currents

Yosef Ashkenazy[1], Eli Tziperman[2], and Francis Nimmo[3]

[1]Department of Solar Energy and Environmental Physics, The Blaustein Institutes for Desert Research, Ben-Gurion University of the Negev, Midreshet Ben-Gurion, Israel, [2]Department of Earth and Planetary Sciences and School of Engineering and Applied Sciences, Harvard University, Cambridge, MA, USA, [3]Department of Earth and Planetary Sciences, University of California Santa Cruz, Santa Cruz, CA, USA

Abstract It has been suggested that the ice shell of Jupiter's moon Europa may drift non-synchronously due to tidal torques. Here we argue that torques applied by the underlying ocean are also important and can result in non-synchronous rotation. The resulting spin rate can be slightly slower than the synchronous angular rate that would have kept the same point of the ice shell facing Jupiter. We develop an ice shell rotation model, driven by ocean stress calculated using a high-resolution state-of-the-art ocean general circulation model, and take into account the viscoelastic deformation of the ice shell. We use the ice shell model results together with observed limits on the ice shell drift speed to constrain ice shell parameters such as effective viscosity, which is currently uncertain by at least four orders of magnitude. Our results suggest, at best, sluggish ice shell convection. Depending on the relaxation time scale of the ice shell and on the ocean currents, the ice shell may exhibit negligible drift, constant drift, or oscillatory drift superimposed on random fluctuations. The expected rotation rate exceeds ∼30 m/yr; future spacecraft observations can be used to test these predictions and yield insight into the properties of the ice shell and underlying ocean.

Plain Language Summary Some icy moons in the solar system, like Jupiter's moon Europa and Saturn's moon Enceladus, are believed to have deep oceans below their ice shell. Such moons, Europa included, may also be tidally locked to their corresponding planet such that the same side of the moon always faces its planet. State-of-the-art oceanic simulations of Europa's ocean exhibit strong upper ocean jets. We propose that these jets can drive its overlying ice shell, to drift slowly from its tidally locked, synchronized rotation state. We develop a mathematical model to study the effects of ocean currents on the overlying ice shell. We show that the ocean currents may cause the ice shell to drift and that future measurements of the drift may be used to estimate key unknown parameters of the ice shell such as its effective viscosity.

1. Introduction

Europa, one of the four Galilean moons of Jupiter, is considered a prime candidate for extra-terrestrial life (Chyba & Phillips, 2001; Hand et al., 2009; Pappalardo et al., 2013) due to its deep (∼100 km) ocean (Carr et al., 1998; Cassen et al., 1979; Kivelson et al., 2000) that underlies a thick ice shell (several to tens of km) (Billings & Kattenhorn, 2005; Carr et al., 1998; Cassen et al., 1979; Hussmann et al., 2002; Tobie et al., 2003). The existence of an ocean under the ice shell is indicated by the observed induced magnetic field (Khurana et al., 1998), observations of ice tectonics (Pappalardo et al., 1999) and perhaps also by water vapor plumes over Europa's mid-southern latitudes (Roth et al., 2014; Sparks et al., 2016).

Europa is tidally locked to Jupiter such that its spin rate (Europa's day is equal to about 3.5 Earth days) is approximately equal to the orbital rotation rate around Jupiter. The maximum possible non-synchronous rotation (NSR) rate was estimated to be ∼1 km yr^{-1} (Hoppa et al., 1999) based on a comparison between Voyager 2 and Galileo spacecraft images that are 17 years apart. There are several hints that Europa rotates non-synchronously. First, the distribution of craters on Europa does not seem to reflect the asymmetry one would expect under complete synchronization, as the leading hemisphere should host more craters in comparison to the trailing hemisphere (Chapman et al., 1998; Shoemaker & Wolfe, 1982). Second, mapping the fine-scale fractures and patterns of Europa's surface has been used to argue for NSR (Geissler et al., 1998; Greenberg et al., 1998; Helfenstein & Parmentier, 1985; McEwen, 1986).

NSR can occur either for the entire moon or for the ice shell separate from the interior (Greenberg & Weidenschilling, 1984; Hoppa et al., 1999). It can be driven by tidal torques associated with the eccentric orbit of Europa that can slightly increase its rotation rate (Hoppa et al., 1999), perhaps combined with slow thermal adjustment of the ice shell (Ojakangas & Stevenson, 1989). However, a sufficiently large mass or shape asymmetry, possibly together with an elastic resistance of its ice shell, can lead to complete phase locking (synchronous rotation) (Goldreich & Mitchell, 2010; Greenberg & Weidenschilling, 1984; Hoppa et al., 1999). If Europa's ocean decouples the rocky core from the ice shell, the shell can display NSR even when the rocky core of Europa is phase locked (Hoppa et al., 1999). Below we focus on the possibility of NSR of the ice shell driven by ocean currents, which has not been investigated in a quantitative fashion hitherto.

Europa's ocean dynamics have been studied using a variety of models and mechanisms (Gissinger & Petitdemange, 2019; Goodman, 2012; Goodman & Lenferink, 2012; Goodman et al., 2004; Melosh et al., 2004; Soderlund et al., 2014; Thomson & Delaney, 2001; Tyler, 2008; Vance & Goodman, 2009), and scaling arguments were used to suggest the existence of alternating zonal jets (Vance & Goodman, 2009). Tides can also excite internal waves (Rovira-Navarro et al., 2019) and libration-driven elliptical instability can also drives ocean motions (Lemasquerier et al., 2017). Recent studies of Europa's ocean (Ashkenazy & Tziperman, 2021; Kang, 2022; Kang et al., 2022; Soderlund, 2019; Soderlund et al., 2014; Zeng & Jansen, 2021) used global models, taking into account elements such as non-hydrostatic effects and the full Coriolis force, to study the ocean dynamics, and reported a wide low-latitude eastward jet, high-latitude westward jets, and a highly turbulent ocean. Negative (westward), upper ocean, low latitude zonal flows have been reported by some previous studies (Ashkenazy & Tziperman, 2021; Kang, 2022; Soderlund et al., 2014) and can be attributed to the thermal-wind relation in which the zonal velocity decreases with height if the density decreases poleward; see Ashkenazy and Tziperman (2021).

The zonal jets at the top of the ocean exert stress on the bottom of the ice shell, which can cause a slow drift of the shell relative to the rocky core. In the present study, we develop a model of ice shell drift that takes into account the influence of oceanic stress on the dynamics of the ice shell, as well as the viscoelastic adjustment of the ice shell itself. We ignore internal ice flow within the shell as this is very slow in comparison to the ice shell drift discussed here (Ashkenazy et al., 2018). By comparing the model predictions to observational constraints, we estimate and constrain parameters of the elastic and viscous responses of the ice shell that are currently very poorly known.

To understand the interaction of the non-synchronous ice shell drift and the viscoelastic response of the shell, we need to consider both the location of the tidal bulge (the direction of the long axis of its ellipsoidal shape) and of some feature (e.g., a crater) on the ice shell surface assumed to initially face Jupiter. First, we consider two limit cases of possible movement of the ice shell in response to an ocean torque: (a) The ice shell is rotated as a rigid body without any deformation of the ice. In that case (the rigid shell case), tidal torques will act to restore the ice shell bulge to face Jupiter, and no elastic restoring force will be active. (b) The ice shell tidal bulge remains facing Jupiter, yet the ice shell itself rotates and deforms such that the location of a crater propagates away from the line connecting the centers of Europa and Jupiter (the flexible shell case). In this case, the net torque due to the tidal forces on the ice shell vanishes (because it acts on the bulge which still faces Jupiter), and only the force due to the ice shell elasticity (Goldreich & Mitchell, 2010) will act to restore the crater to its original location. In reality, both forces (tidal and elastic) act on the ice shell. Since the tidal force is much larger than the elastic force (Goldreich & Mitchell, 2010), the tidal bulge of the ice shell remains facing Jupiter. However, as long as the shell is sufficiently flexible, it can rotate under the influence of ocean torques while conforming its shape to the tidal bulge that remains facing Jupiter. We thus assume below that the tidal bulge faces Jupiter and ignore the tidal force in our subsequent calculations.

In the above, we did not consider the viscous effects of the ice, which may affect the NSR of the ice shell as follows. In the absence of viscous effects, if the ice shell is initially rotated by an ocean torque, elastic torques will attempt to return the crater to its original position, and the shape will be restored such that the tidal bulge is back at the crater's position. However, viscous ice adjustment means that the bulge relaxes to its new position relative to the crater (Greenberg & Weidenschilling, 1984), which weakens the elastic force with time, such that the deformed ice will not return to its original shape. The ocean torque can now lead to a further motion of the crater and again to a viscous adjustment to the new position. This amounts to a slow drift of the crater location in response to a continuous torque due to ocean currents. The speed of the drift depends on the viscous adjustment/relaxation time scale of the ice (Greenberg & Weidenschilling, 1984)—faster drift when the viscous time scale is short.

2. Methods and Model

2.1. Ocean Simulations and the Calculation of the Ocean Torque

The ocean simulations are two-dimensional (latitude-depth) and were performed using the MITgcm, a state-of-the-art oceanic general circulation model (Marshall et al., 1997; MITgcm Group, 2021). We use no-slip boundary conditions at the bottom and at the ocean-ice interface, with and without a linear drag term applied at the ocean top and bottom levels. The meridional resolution is 1/24 of a degree latitude (1.1 km) spanning a meridional range from 70°S to 70°N. There are 100 vertical levels with thicknesses from 25 m near the top to 1,150 m at the bottom where the overall depth of the ocean is 100 km. We use the shelf ice package of MITgcm (Losch, 2008) to represent a 10 km thick ice shell. The surface temperature is prescribed following Ashkenazy (2018). The eddy coefficients follow the choices of Ashkenazy and Tziperman (2021) where the horizontal eddy diffusion for temperature and salinity is 30 $m^2\ s^{-1}$, the horizontal viscosity is 300 $m^2\ s^{-1}$, the vertical diffusion is $10^{-4}\ m^2\ s^{-1}$, and the vertical viscosity is $10^{-3}\ m^2\ s^{-1}$. The ocean linear friction coefficient $\tilde{r}_o$ is set to 2×10^{-4} m s^{-1}, a typical value used in Earth's ocean modeling (Marshall et al., 1997; MITgcm Group, 2021); we also used a three times higher linear friction coefficient of $\tilde{r}_o = 6\times10^{-4}$ m s^{-1} to verify the sensitivity of the results to this parameter.

Using the output of the ocean model, we calculate the zonal stress on the ice shell as follows,

$$\begin{aligned}\tau_\lambda(\lambda,\phi) &= -\rho_o\left(\nu_z+\tilde{r}_o\frac{\Delta z}{2}\right)\left.\frac{\partial u}{\partial z}\right|_{z=0}\\ &\approx -\rho_o\left(\nu_z+\tilde{r}_o\frac{\Delta z}{2}\right)\frac{R\omega\cos\phi-u(z=-\Delta z/2)}{\Delta z/2}\end{aligned} \tag{1}$$

where the second line uses the finite difference approximation of the vertical shear, taking the difference between the surface ocean velocity which is equal to that of the ice shell (no-slip condition), and the ocean velocity in the middle of the uppermost ocean level, $\Delta z/2$. Also, λ is the longitude, ϕ is the latitude, $\rho_o = 1{,}046$ kg m^{-3} is the ocean water density, ν_z is the oceanic vertical viscosity coefficient, ω the angular velocity of the ice shell, and $R = 1{,}561$ km is the radius of Europa. The stress τ_λ is used to calculate the torque in the z direction (parallel to the rotation axis) using an integral of the zonal stress τ_λ times the distance from the axis of rotation ($R\cos\phi$), integrated over the surface area within the model domain,

$$\frac{M_z}{I} = \frac{R^3}{I}\int \tau_\lambda\cos^2\phi\, d\phi\, d\lambda = r_o(\omega_o-\omega) \tag{2}$$

where

$$r_o = \frac{16\pi R^4\rho_o}{3I\Delta z}\left(\nu_z+\tilde{r}_o\frac{\Delta z}{2}\right), \tag{3}$$

$$\omega_o = \frac{3}{8\pi R}\int u\left(z=-\frac{\Delta z}{2}\right)\cos^2\phi\, d\phi\, d\lambda. \tag{4}$$

Then the torque is multiplied by an appropriate constant—$24\times360 = 8{,}640$ in our case as the model's resolution is 1/24 of a degree—to represent the torque applied by a 360° longitude ocean. We calculate the moment of inertia of the ice shell as $I = 8\pi\rho_i R^5(1-\alpha^5)/15 = 4.5\times10^{32}$ kg m^2, where $\alpha = (R-H_{\text{ice}})/R$, the ice shell density is $\rho_i = 917$ kg m^{-3}, and $H_{\text{ice}} = 10$ km. The uncertainty of the latter value is comparable to the ice thickness itself. Following Equation 3, in the absence of linear drag in the ocean, $r_o \sim 9.2\times10^{-9}\ s^{-1}$ while the value is higher when the oceanic drag coefficient is taken into account; that is, $r_o \sim 3.2\times10^{-8}\ s^{-1}$ when using a standard ocean linear drag of $\tilde{r}_o = 2\times10^{-4}$ m s^{-1} and $r_o \sim 7.9\times10^{-8}\ s^{-1}$ when using a three times larger ocean linear drag of $\tilde{r}_o = 6\times10^{-4}$ m s^{-1}. We note that different linear drag coefficients $\tilde{r}_o$ result in different surface currents and thus different forcing; thus the friction coefficient r_o cannot be altered without altering the ocean forcing ω_o. However, our results show that all simulations with and without oceanic drag $\tilde{r}_o$ yield similar constraints on τ. We note that we performed only three, 2D, oceanic simulations to estimate the torque due to ocean currents, and found that all resulted in similar retrograde drift; by retrograde drift, we are referring to the ice shell spinning slightly slower than the synchronous angular rate that would have kept the same point of the ice shell facing Jupiter. This retrograde flow is consistent with previous studies (Ashkenazy & Tziperman, 2021; Kang, 2022; Soderlund et al., 2014) that reported westward flow at the upper ocean of the low latitudes.

Figure 1. A schematic showing the Europa ice shell on the left and Jupiter on the right, with the angle θ appearing in the model Equation 5. We assume that $\lambda = 0$.

Given the two-dimensional geometry of the model, the torque due to the meridional flow τ_ϕ vanishes due to symmetry. That is, meridional stress (say due to a poleward surface flow in the northern hemisphere) implicitly exists at all longitudes. When this stress is integrated over the ocean surface, the net poleward torque therefore vanishes (the poleward stress at any longitude is canceled by an equal contribution at a longitude 180° away). Thus the ocean model used here cannot represent meridional ocean torques on the ice shell.

2.2. Model for the Ice Shell Drift Rate

In the model proposed here, the position of the ice shell is represented by an angle θ between a fixed location on the equatorial plane of Europa's ice shell (e.g., the location of a crater) and the axis connecting the centers of Jupiter and Europa, see Figure 1. We assume, based on Goldreich and Mitchell (2010), that the tidal torque is much larger than the elastic torque such that the tidal bulge raised by Jupiter is facing Jupiter with no offset, that is, $\lambda = 0$ in Figure 1. In that case, the momentum equation that describes the motion of the ice shell is,

$$\begin{aligned} \frac{d^2\theta}{dt^2} + F_e &= \frac{M_z}{I} = r_o\left(\omega_o - \frac{d\theta}{dt}\right) \\ F_e &= k_i\left[\theta(t) - \frac{1}{\tau}\int_{-\infty}^{t}\theta(t')e^{(t'-t)/\tau}dt'\right], \end{aligned} \tag{5}$$

where M_z [Equation 2], r_o [Equation 3], and ω_o [Equation 4] are defined in the previous subsection. The ocean torque is written as the friction coefficient times the difference between the shell rotation rate and the effective ocean angular velocity. A viscoelastic force due to the ice shell drift is denoted F_e and involves a characteristic viscous time scale τ over which the ice loses its elasticity; this form is similar to the integral form of the Maxwell model (Morrison, 2001). When the ice viscous adjustment time τ is very long, the ice remains elastic and $F_e = k_i\theta$, where k_i describes the elastic response of the ice shell and is independent of shell thickness [Equation 10]. When τ is very small, the ice loses its elasticity very quickly, such that in practice, there is no elastic force and $F_e = 0$.

Equation 5 can be converted into the second-order ordinary differential Equation 6 for the ice drift rate $\omega = d\theta/dt$, which is more convenient to analyze and has the mathematical form of that for a forced and damped harmonic oscillator (except that it is written for the angular velocity rather than for the angle, see Section 2.3). The model's parameters and forcing can be estimated using the current knowledge of Europa's ice shell and results from the ocean simulations (Sections 2.1 and 2.4).

2.3. Solution for the Ice Shell Drift Rate

It is easier to solve and analyze the integrodifferential model Equation 5 after converting it to an ordinary differential equation. This is achieved by taking the time derivative of the second equation of Equation 5, using integration by parts and the Leibniz rule. This leads to a single 2nd-order ordinary differential equation where for the angular velocity of the ice shell ($\omega = d\theta/dt$),

$$\frac{d^2\omega}{dt^2} + \left(r_o + \frac{1}{\tau}\right)\frac{d\omega}{dt} + \left(k_i + \frac{r_o}{\tau}\right)\omega = r_o\left(\frac{\omega_o}{\tau} + \frac{d\omega_o}{dt}\right). \tag{6}$$

The general solution of the above equation is a sum of a particular solution and the general solution of the homogeneous part. The solution of the homogeneous part of the equation is that of the damped harmonic oscillator (although, again, this equation is for the angular velocity rather than angle as is the case in the standard damped harmonic oscillator), for which ω decays exponentially in time from its initial conditions. The particular solution of the equation for time-independent forcing, $d\omega_o/dt = 0$ is,

$$\omega = \frac{r_o\,\omega_o}{k_i\tau + r_o}, \tag{7}$$

where this is also the steady state solution of the model [Equation 6], that is, $d\omega/dt = 0$. Thus, the rate of the ice drift is reduced by the elastic and viscosity parameters $k_i\tau$. Given the decay of the homogeneous solution, the

system's initial conditions do not matter beyond the decay time of the homogeneous equation. We note that the time derivative of the forcing $d\omega_o/dt$ in the RHS of Equation 6 has a very minor role in the solution.

The frequency spectrum of the ice shell movement for the case of general forcing, $\omega_o(t)$, ignoring the transient decay, can be derived by taking the Fourier transform of Equation 6 and multiplying by its complex conjugate,

$$|\hat{\omega}(\nu)|^2 = \frac{|\hat{f}(\nu)|^2}{(k_i + r_o/\tau)^2 + \left(r_o^2 + \tau^{-2} - 2k_i\right)\nu^2 + \nu^4}, \tag{8}$$

where $|\hat{f}(\nu)|^2$ is the power spectrum of the forcing $r_o(\omega_o/\tau + d\omega_o/dt)$ and ν is the frequency. When the forcing is a Gaussian white noise $f(t) = A\xi_t$, $|\hat{f}(\nu)|^2 = (2\pi A)^2\left(1/\tau^2 + \nu^2\right)$ and the power spectrum can be found using Equation 8. In this case, the extrema points of the power spectrum can be found where one extremum point is at the zero frequency and the other at,

$$(\nu^*)^2 = -\frac{1}{\tau^2} + k_i\sqrt{1 + \frac{2r_o}{k_i\tau} + \frac{2}{k_i\tau^2}}. \tag{9}$$

When the argument of the square root is positive, the maximum of the power spectrum (resonance) is at non-zero frequency; otherwise, the maximum of the power spectrum is at zero, and there is no resonance.

2.4. Estimating the Elastic and Viscous Parameters of the Ice Shell

It is possible to estimate the elastic constant of the ice, k_i appearing in our ice shell model (5), based on Equation 9 of Goldreich and Mitchell (2010),

$$k_i = \frac{24(1+\nu)(1+k_f)^2 q^2 \mu}{5(5+\nu)\rho_i R^2}. \tag{10}$$

The definitions and details on the parameters (explanation and estimated value) can be found in Goldreich and Mitchell (2010) and the estimated value is $k_i \approx 2.5 \times 10^{-12}\ \mathrm{s}^{-2}$. Note that in the thin shell limit, k_i does not depend on the shell thickness, because both the elastic torque and the mass of the shell depend linearly on this quantity. If the ice shell is convecting, k_i will be reduced by a factor of the elastic thickness divided by the total shell thickness. This will tend to increase the NSR rate [Equation 7]. The uncertainties on other parameters in this expression are small, except for the rigidity μ. Here we follow (Goldreich & Mitchell, 2010) and assume that the relevant rigidity is that of intact ice.

The viscous relaxation (Maxwell) time scale τ can be estimated by dividing typical ice dynamical viscosity η by μ, the ice shell rigidity. The estimated uncertainty range for τ is quite large. In the case of convecting ice η can be estimated as the melting viscosity, which ranges between 10^{13}–10^{15} Pa s (Goldsby & Kohlstedt, 2001). When the ice is not convecting, the viscosity varies with depth and is much larger near the surface of the ice, due to the lower temperature there.

Calculation of the viscous relaxation timescale, in this case, is not straightforward. In this pilot study, we simply choose an effective upper limit shell viscosity of 10^{17} Pa s to represent the logarithmic mean of the viscosity (near-surface ice is sufficiently cold and brittle that it will not contribute to viscoelastic processes). Less simplistic calculations of the relaxation timescale for realistic ice shell structures should certainly be attempted in the future. For now, we take the overall range of η to be $10^{13} - 10^{17}$ Pa s and accordingly

$$\tau = \frac{\eta}{\mu} \sim 2.5 \times 10^3 \mathrm{s} - 2.5 \times 10^7 \mathrm{s}.$$

3. Results

We consider several scenarios of oceanic forcing on the ice shell: (a) a constant torque, (b) a periodic torque due to the equatorward propagation of Taylor columns outside the tangent cylinder (Ashkenazy & Tziperman, 2021) that lead to periodic changes in surface ocean currents, (c) a stochastic torque due to the transient nature of the oceanic flow, and (d) an ocean-model-derived forcing. The actual ocean torque (d) is a combination of the first three cases.

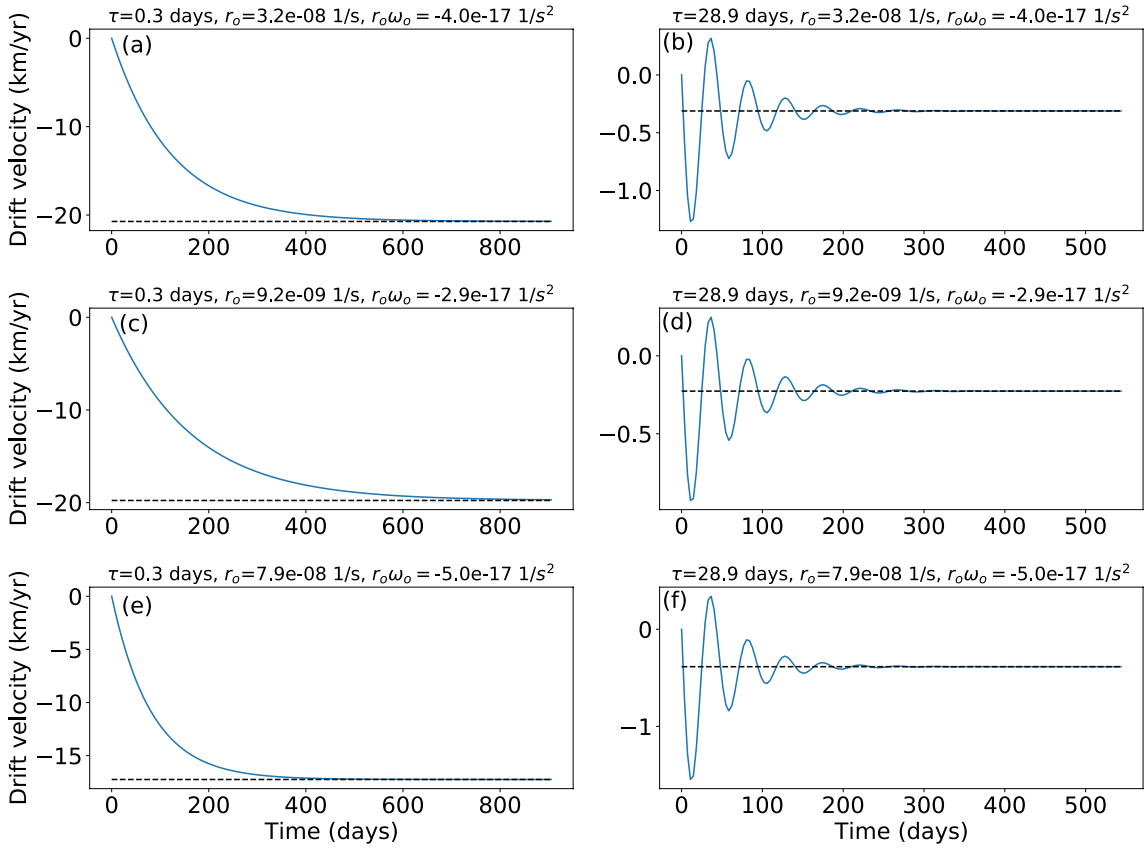

Figure 2. Time series of the ice drift velocity versus time for the case of a constant ocean torque, showing the adjustment starting from zero initial conditions. (a) Exponential decay parameter regime for short ice relaxation time scale of 0.3 days, (b) oscillatory regime for long ice relaxation time scale of ≈30 days. Panels a and b depict the time series when the linear drag is included in the ocean model (the corresponding ice friction coefficient is $r_o = 3.2 \times 10^{-8}$ s^{-1}), panels c and d depict the time series for the case of ocean simulation without the linear drag (for which the ice friction coefficient is $r_o = 9.2 \times 10^{-9}$ s^{-1}), and panels e and f depict the time series for the case of ocean simulation with large linear drag (for which the ice friction coefficient is $r_o = 7.9 \times 10^{-8}$ s^{-1}). The observational upper bound on the drift velocity is 1 km yr^{-1} (Hoppa et al., 1999).

3.1. Constant Ocean Forcing

Assume first that the effective ocean angular velocity is constant in time (ocean currents are in a steady state). The steady-state solution for the angular velocity of the ice-shell drift, ω, under constant ocean torque forcing (i.e., ω_o = const) is given in Equation 7. The ice shell rate of drift is proportional to the ocean forcing ω_o. An increase in k_i or τ leads to a smaller drift rate; in particular, a longer relaxation timescale (larger τ) would reduce the drift rate. Note that k_i is proportional to ice rigidity μ while η is proportional to $1/\mu$ such that $k_i\tau$ appearing in the denominator of Equation 7 should be independent of μ. When starting from arbitrary initial conditions, the adjustment to the constant drift solution (Figure 2) involves either an exponential decay to the steady state or oscillations whose amplitude decays exponentially. Oscillations occur (Figures 2b, 2d, and 2f) when the time scale τ is large, with a frequency $\sqrt{k_i - (r_o + 1/\tau)^2/4}$; when the argument under the square root is negative (for small τ), exponential decay occurs (Figures 2a, 2c, and 2e). This damped internal oscillatory behavior plays an important role when the ocean forcing is periodic or stochastic, as discussed next.

The shell relaxation time scale, τ, can drastically affect the ice-drift velocity, as its uncertainty spans at least four orders of magnitude (from 1 hr to hundreds of days). The resulting ice shell drift velocity ranges from a few tens of meters per year to almost one hundred km per year (Figure 3a). Observational constraints (Hoppa et al., 1999) indicate that the ice-shell velocity is smaller than 1 km yr^{-1} (dashed line in Figure 3a) and this upper limit constrains the shell relaxation time scale to be larger than about 10 days, for all simulations of different oceanic linear drag. Conversely, unless the effective ice shell viscosity exceeds 10^{17} Pa s, which would only occur for a non-convecting shell (McKinnon, 1999), we expect a NSR period of $\lesssim 3 \times 10^5$ yrs (Figure 3a) or a drift velocity larger than about 30 m yr^{-1}. Such a drift period would be readily detectable with a future mission to Europa.

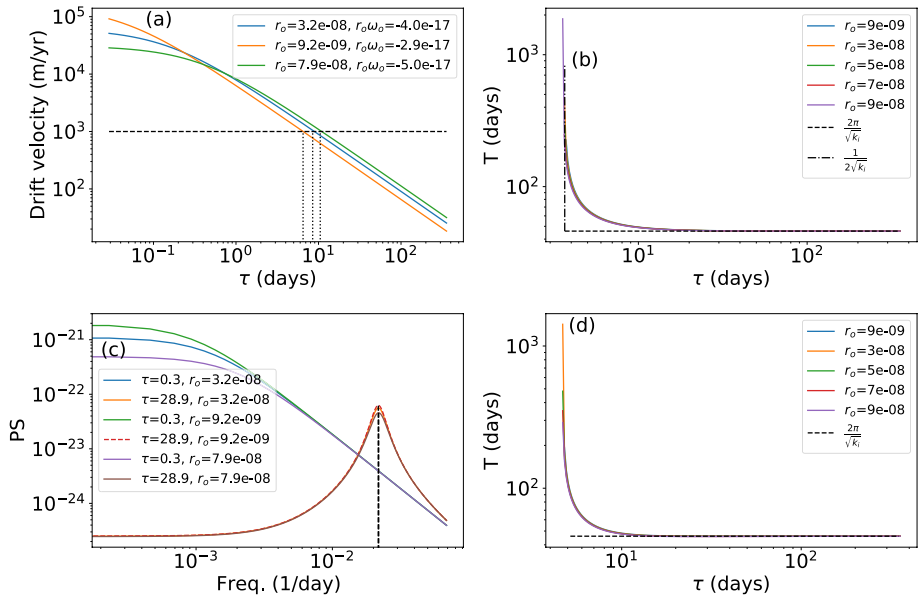

Figure 3. Parameter sensitivity. (a) Steady-state solution for drift velocity as a function of τ for a constant ocean torque for three cases, with (blue) standard oceanic drag ($\tilde{r}_o = 2 \times 10^{-4}$ m s^{-1}, $r = 3.2 \times 10^{-8}$ 1 s^{-1}), without (orange) oceanic linear drag ($\tilde{r}_o = 0$, $r = 9.2 \times 10^{-9}$ 1 s^{-1}), and with large (green) ocean linear drag ($\tilde{r}_o = 6 \times 10^{-4}$ m s^{-1}, $r = 7.9 \times 10^{-8}$ s^{-1}). The corresponding oceanic torque $r_o\omega_o$ is indicated in the figure legend. The dashed line shows the observationally constrained upper limit of the ice shell drift velocity of 1 km yr^{-1} (Hoppa et al., 1999), indicating that τ should be larger than ∼10 days, for all cases; the vertical dotted lines indicate the minimal τ of the different cases. (b) Oscillation period (T, see Figure 2b) as a function of τ for a constant ocean torque and five friction coefficient, r_o, values. The oscillation period converges to ∼45 days for realistic τ that is larger than ∼10 days. (c) Power spectra of the drift velocity as a function of frequency for different model parameters for the stochastic forcing case, corresponding to the cases shown in panel a. (d) Period corresponding to the spectral peak under stochastic forcing as a function of τ. Also here, the period converges to ∼45 days, as for the constant forcing case shown in panel b.

In Figure 3b, we present the period of the internal oscillations of the ice shell $\left(\text{i.e., } 2\pi/\sqrt{k_i - (r_o + 1/\tau)^2/4}\right)$ as a function of the shell relaxation time scale, τ, and ocean friction parameter, r_o. We show that r_o hardly affects the period for realistic values of r_o while the relaxation time scale, τ, can have a much larger effect on the period. Given the constraint that $\tau \gtrsim 10$ days, the oscillation period (Figure 3b) is nearly independent of the actual value of τ and converges to $T \sim 2\pi/\sqrt{k_i} \approx 45$ days; the oscillation period depends mainly on the shell rigidity, while the mean drift rate depends on τ.

3.2. Periodic Forcing

We assume, for simplicity, that $\omega_o(t)$ is a pure cosine function. The solution of Equation 6 is periodic with the same period as the forcing, and resonance is obtained when the forcing frequency equals $(\nu^*)^2 = -1/\tau^2 + k_i\sqrt{1 + (2r_o)/(k_i\tau) + 2/(k_i\tau^2)}$. For large enough τ, $\nu^* = \sqrt{k_i}$. Note that the resonance frequency is related to, but not identically equal to, the frequency of the damped internal oscillations given above.

3.3. Stochastic Forcing

The power spectrum of the drift can be evaluated for a general forcing [Equation 8]. There are two types of responses to a white noise forcing, one with a spectral peak at the resonance frequency ν^* (on the right side of Figure 3c), and another with a monotonically decreasing Lorentzian-like power spectrum with increasing frequency, showing a transition from a plateau at low frequencies to a power-law decay for higher frequencies. The transition (crossover) point (∼1,000 days) indicates the expected time scale of the forced stochastic variability of the ice shell drift. As before, the numerical value of the ocean friction coefficient, r_o, does not significantly affect the spectra within its range of uncertainty, for realistic values of τ. Variations of the ice relaxation time scale τ within its own range of uncertainty results in the above two different types of spectra. In Figure 3d we plot the

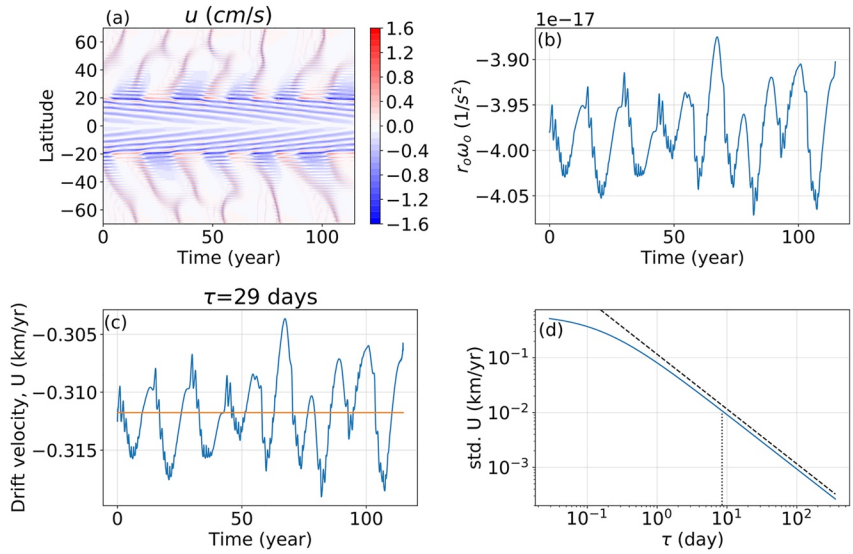

Figure 4. Ice shell drift forcing and response: (a) The ocean zonal velocity (cm/s) as a function of time (in years) and latitude. Note the difference between the equatorward propagating Taylor columns outside the tangent cylinder (20°S–20°N) and the periodic pattern within the tangent cylinder (Ashkenazy & Tziperman, 2021). Note also the westward flow of the equatorial current. (b) The global average of the zonal torque due to ocean currents, $r_o\omega_o$, as a function of time. (c) Blue line: drift velocity of a point on the equator of Europa (km/year). Orange line: the ice-shell drift velocity when forcing the model by the constant temporal mean ocean torque. Here $\tau = 29$ days. (d) The standard deviation of the ice-shell drift velocity as a function of the relaxation time scale τ. The std decreases like $1/\tau$ (dashed line) for large τ.

period at the resonance frequency for the uncertainty range of τ and r_o. Different values of τ can result in very different periods of the spectral peak, from about 50 to 1,000 days. Since τ should be larger than about 10 days to satisfy the ice drift constraint of Hoppa et al. (1999), one expects the spectral peak of the ice shell drift rate oscillations due to white noise stochastic forcing to be around 45 days. The expected magnitude of these oscillations depends on the magnitude of the stochastic forcing; as discussed below in the context of the solution driven by the ocean model solution, the oscillations are expected to be small.

3.4. The Ocean-Model-Derived Forcing Case

Figure 4c shows the ice-shell drift velocity for the ocean torque forcing derived from our ocean model, shown in Figure 4b; linear oceanic drag was included in this simulation (corresponding to an ice model friction coefficient of $r_o = 3.2 \times 10^{-8}$ s^{-1}). The results for the oceanic simulation in the absence of linear oceanic drag (corresponding to an ice model friction coefficient of $r_o = 9.2 \times 10^{-9}$ s^{-1}) and with a large linear oceanic drag (corresponding to an ice model friction coefficient of $r_o = 7.9 \times 10^{-8}$ s^{-1}) are presented in Supporting Information S1 (Figures S1 and S2). This solution combines features from the above-mentioned constant, periodic, and stochastic forcing scenarios. The power spectrum of the forcing (Figure S3 in Supporting Information S1) shows a strong peak at about 10 years resulting from the speed of propagation of the Taylor columns, indicating that the forcing is nearly periodic. This ∼10 yr period is much larger than the resonance period of ∼45 days discussed above (Figure 3d), and we, therefore, do not expect a resonant response or a peak in the NSR drift spectrum due to the ocean current forcing. Moreover, the noisy fluctuations superimposed on the nearly periodic ocean torque forcing are relatively small (as seen by the tails of the 10-year peak of the power spectrum). As a result, a resonance due to this noisy part of the forcing is likely to be negligible relative to the response to the oscillatory part of the forcing. As τ increases, the standard deviation of the ice shell drift fluctuations driven by the deviations of the ocean model torque from its long-term mean decreases like $1/\tau$ (dashed line in Figure 4d). Given the observational constraint of $\tau > 10$ days, Figure 4d shows that the ice shell movements due to this time-variable ocean forcing are expected to be very small (standard deviation <10 m yr^{-1}). Since the drift rate, ω [Equation 7] is proportional to $1/\tau$ (i.e., $\omega \approx r_o\omega_o/(k_i\tau)$ for $k_i\tau \gg r_o$), the ratio between the standard deviation and the mean of the drift rate ω is expected to remain constant for large τ. We conclude that the time-averaged ocean torque is expected to dominate the ice-shell drift rate, resulting in steady drift. Since $\tau \gtrsim 10$ days (∼10^6 s) is required by the observations (Figure 3a), the

effective ice shell viscosity must exceed about 3×10^{15} Pa s. Although this effective viscosity will only roughly correspond to the interior viscosity of a convecting ice shell, a value of 3×10^{15} Pa s may imply that at best sluggish convection is occurring (McKinnon, 1999).

4. Discussions

A surprising result of our model is that the torque calculated by the ocean model is negative and thus decreases the ice shell rotation rate relative to the synchronous rotation case. This is in contrast to the effect of tidal forcing which tends to increase the rotation rate (Hoppa et al., 1999). It has been shown that tectonic crack orientations can equally well be explained by retrograde NSR as by prograde NSR (Sarid et al., 2004), so either possibility is currently viable based on existing observations.

One way of detecting NSR is to look for offsets between the predicted and observed location of the terminator (the line separating the daylight and night side) (Hoppa et al., 1999). Some of the best *Galileo* images of the terminator have a resolution of 0.4 km (Hoppa et al., 1999). Future spacecraft observations are likely to have resolutions significantly better than this. Assuming a time interval of 30 years between the *Galileo* observations and future imaging campaigns, a terminator location with a precision of 0.4 km implies that an NSR period of about 7×10^5 years (drift rate of 15 m yr^{-1}) would be marginally detectable, larger than our estimate for the slowest ice-shell drift of ∼30 m yr^{-1}.

The model we developed for the ice shell drift is highly simplified. Moreover, it relies on the oceanic general circulation model we use, whose parameters are partially based on Earth's ocean parameters (like the vertical viscosity and linear drag coefficient) and hence uncertain in the context of Europa. While we have demonstrated that the general conclusion of retrograde drift is insensitive to some of the main model parameters (like the linear drag), one cannot rule out the possibility that sensitivity to the ocean model setup and other parameters (such as the distribution of bottom heating) won't cause an opposite drift, implying a non-negligible uncertainty in the magnitude and sign of our estimated drift velocity.

Another effect that was not included in the proposed model is the effect of a tidal phase lag on the drift of the ice shell. Such a lag would impose an additional torque tending to spin the satellite up (Goldreich & Mitchell, 2010). However, the size of the lag for Europa is expected to be small, <0.3° for a shell thickness <30 km (Moore & Schubert, 2000), and as a result, we estimate this torque to be smaller than the ocean torque, although certainly not negligible. See the Supporting Information S1 for an estimate of this torque and additional discussion.

Further work is needed to understand whether tidal or ocean torques will dominate. 3D simulations of Europa without linear drag are highly turbulent (Ashkenazy & Tziperman, 2021) and result in super-rotation (eastward flow) at the upper, low latitude, ocean; yet, our preliminary 3D simulation with linear drag indicates that the flow is negative (westward). Moreover, this preliminary simulation exhibits a periodicity of ∼50 days (most probably due to eddy and convection dynamics) which may resonate with the internal ice dynamics reported here. The ocean eddies are expected to add to the amplitude and change the spectral characteristics of the stochastic forcing experienced by the ice shell. The computational cost of 3D eddy-resolving simulations prohibits obtaining a sufficiently long time series of ocean torques to be used to drive the ice shell model drift equation used here. Apart from our use of a 2D ocean model, other significant assumptions include a single viscoelastic adjustment time scale and neglect of tidal forcing. Our drift rate predictions, which depend primarily on the viscoelastic relaxation timescale τ (Figure 3a) are necessarily uncertain because of uncertainty in τ. Yet the constraint of $\tau \gtrsim 10$ days indicates that the effective ice shell viscosity should be $\eta \gtrsim 3 \times 10^{15}$ Pa s.

5. Conclusions

The model suggested here demonstrates how the combination of ocean torques due to zonal surface currents and viscous adjustment of the ice shell may lead to a potentially observable, retrograde non-synchronous drift (Figure 3a). Oscillatory or stochastic rotation rate variations are expected to be minor, ruling out potential confusion with long-period librations (Rambaux et al., 2011). Future missions and observations are expected to lead to an improved constraint on the ice shell drift velocity. The expected precision is about 15 m yr^{-1} or better, smaller than our anticipated slowest drift rate of 30 m yr^{-1}. Using the model developed here, such closer bounds can lead to a tighter constraint on the viscous response time of the ice shell, which plays a dominant role here. Conversely,

a tighter constraint on this ice shell viscous response due to a better understanding of the physics affecting this time scale (ice crystal size, brittle failure, the temperature distribution within the ice, etc.) would permit inferences of Europa's ocean currents.

Conflict of Interest

The authors declare no conflicts of interest relevant to this study.

Data Availability Statement

The model presented in this paper is based on surface ocean currents that were simulated using the MITgcm (MITgcm Group, 2021). Additional information regarding these simulations can be found in Ashkenazy and Tziperman (2021) and the setup files of the numerical simulations can be downloaded from https://doi.org/10.17605/OSF.IO/SVXBQ. The simulated upper ocean zonal currents presented in Figure 4a can be downloaded from https://osf.io/svxbq/files/osfstorage/63d655ad34869301e90b5505.

Acknowledgments
We thank Roiy Sayag for helpful discussions. This work was funded by the Bi-National US-Israel Science Foundation (Grant 2018152), ET was funded by DOE Grant DE-SC0023134, and thanks the Weizmann Institute for its hospitality during parts of this work.

References

Ashkenazy, Y. (2018). The surface temperature of Europa. *Heliyon*, *5*(6), e01908. https://doi.org/10.1016/j.heliyon.2019.e01908
Ashkenazy, Y., Sayag, R., & Tziperman, E. (2018). Dynamics of the global meridional ice flow of Europa's icy shell. *Nature Astronomy*, *2*(1), 43–49. https://doi.org/10.1038/s41550-017-0326-7
Ashkenazy, Y., & Tziperman, E. (2021). Dynamic Europa ocean shows transient Taylor columns and convection driven by ice melting and salinity. *Nature Communications*, *12*(1), 1–12. https://doi.org/10.1038/s41467-021-26710-0
Billings, S. E., & Kattenhorn, S. A. (2005). The great thickness debate: Ice shell thickness models for Europa and comparisons with estimates based on flexure at ridges. *Icarus*, *177*(2), 397–412. https://doi.org/10.1016/j.icarus.2005.03.013
Carr, M. H., Belton, M. J., Chapman, C. R., Davies, M. E., Geissler, P., Greenberg, R., et al. (1998). Evidence for a subsurface ocean on Europa. *Nature*, *391*(6665), 363–365. https://doi.org/10.1038/34857
Cassen, P., Reynolds, R. T., & Peale, S. (1979). Is there liquid water on Europa? *Geophysical Research Letters*, *6*(9), 731–734. https://doi.org/10.1029/gl006i009p00731
Chapman, C., Merline, W., Bierhaus, B., Brooks, S., & Team, G. I. (1998). Cratering in the Jovian system: Intersatellite comparisons. In *Lunar and planetary science conference*.1927.
Chyba, C. F., & Phillips, C. B. (2001). Possible ecosystems and the search for life on Europa. *Proceedings of the National Academy of Sciences of the United States of America*, *98*(3), 801–804. https://doi.org/10.1073/pnas.98.3.801
Geissler, P., Greenberg, R., Hoppa, G., Helfenstein, P., McEwen, A., Pappalardo, R., et al. (1998). Evidence for non-synchronous rotation of Europa. *Nature*, *391*(6665), 368–370. https://doi.org/10.1038/34869
Gissinger, C., & Petitdemange, L. (2019). A magnetically driven equatorial jet in Europa's ocean. *Nature Astronomy*, *3*(5), 401–407. https://doi.org/10.1038/s41550-019-0713-3
Goldreich, P. M., & Mitchell, J. L. (2010). Elastic ice shells of synchronous moons: Implications for cracks on Europa and non-synchronous rotation of Titan. *Icarus*, *209*(2), 631–638. https://doi.org/10.1016/j.icarus.2010.04.013
Goldsby, D., & Kohlstedt, D. (2001). Superplastic deformation of ice: Experimental observations. *Journal of Geophysical Research*, *106*(B6), 11017–11030. https://doi.org/10.1029/2000jb900336
Goodman, J. C. (2012). Tilted geostrophic convection in icy world oceans caused by the horizontal component of the planetary rotation vector. In *American geophysical union, fall meeting 2012, abstract* (pp. P51A–P2017).
Goodman, J. C., Collins, G. C., Marshall, J., & Pierrehumbert, R. T. (2004). Hydrothermal plume dynamics on Europa: Implications for chaos formation. *Journal of Geophysical Research*, *109*(E3), E03008. https://doi.org/10.1029/2003je002073
Goodman, J. C., & Lenferink, E. (2012). Numerical simulations of marine hydrothermal plumes for Europa and other icy worlds. *Icarus*, *221*(2), 970–983. https://doi.org/10.1016/j.icarus.2012.08.027
Greenberg, R., Geissler, P., Hoppa, G., Tufts, B. R., Durda, D. D., Pappalardo, R., et al. (1998). Tectonic processes on Europa: Tidal stresses, mechanical response, and visible features. *Icarus*, *135*(1), 64–78. https://doi.org/10.1006/icar.1998.5986
Greenberg, R., & Weidenschilling, S. J. (1984). How fast do Galilean satellites spin? *Icarus*, *58*(2), 186–196. https://doi.org/10.1016/0019-1035(84)90038-1
Hand, K., Chyba, C., Priscu, J., Carlson, R., & Nealson, K. (2009). Astrobiology and the potential for life on Europa. *Europa*, 589–629.
Helfenstein, P., & Parmentier, E. (1985). Patterns of fracture and tidal stresses due to nonsynchronous rotation: Implications for fracturing on Europa. *Icarus*, *61*(2), 175–184. https://doi.org/10.1016/0019-1035(85)90099-5
Hoppa, G., Greenberg, R., Geissler, P., Tufts, B. R., Plassmann, J., & Durda, D. D. (1999). Rotation of Europa: Constraints from terminator and limb positions. *Icarus*, *137*(2), 341–347. https://doi.org/10.1006/icar.1998.6065
Hussmann, H., Spohn, T., & Wieczerkowski, K. (2002). Thermal equilibrium states of Europa's ice shell: Implications for internal ocean thickness and surface heat flow. *Icarus*, *156*(1), 143–151. https://doi.org/10.1006/icar.2001.6776
Kang, W. (2022). Different ice-shell geometries on Europa and Enceladus due to their different sizes: Impacts of ocean heat transport. *The Astrophysical Journal*, *934*(2), 116. https://doi.org/10.3847/1538-4357/ac779c
Kang, W., Mittal, T., Bire, S., Campin, J.-M., & Marshall, J. (2022). How does salinity shape ocean circulation and ice geometry on Enceladus and other icy satellites? *Science Advances*, *8*(29), eabm4665. https://doi.org/10.1126/sciadv.abm4665
Khurana, K., Kivelson, M., Stevenson, D., Schubert, G., Russell, C., Walker, R., & Polanskey, C. (1998). Induced magnetic fields as evidence for subsurface oceans in Europa and Callisto. *Nature*, *395*(6704), 777–780. https://doi.org/10.1038/27394
Kivelson, M. G., Khurana, K. K., Russell, C. T., Volwerk, M., Walker, R. J., & Zimmer, C. (2000). Galileo magnetometer measurements: A stronger case for a subsurface ocean at Europa. *Science*, *289*(5483), 1340–1343. https://doi.org/10.1126/science.289.5483.1340

Lemasquerier, D., Grannan, A., Vidal, J., Cébron, D., Favier, B., Le Bars, M., & Aurnou, J. (2017). Libration-driven flows in ellipsoidal shells. *Journal of Geophysical Research: Planets*, *122*(9), 1926–1950. https://doi.org/10.1002/2017je005340

Losch, M. (2008). Modeling ice shelf cavities in a z-coordinate ocean general circulation model. *Journal of Geophysical Research*, *113*(C8), C08043. https://doi.org/10.1029/2007jc004368

Marshall, J., Adcroft, A., Hill, C., Perelman, L., & Heisey, C. (1997). A finite-volume, incompressible Navier Stokes model for studies of the ocean on parallel computers. *Journal of Geophysical Research*, *102*(C3), 5753–5766. https://doi.org/10.1029/96jc02775

McEwen, A. S. (1986). Tidal reorientation and the fracturing of Jupiter's moon Europa. *Nature*, *321*(6065), 49–51. https://doi.org/10.1038/321049a0

McKinnon, W. B. (1999). Convective instability in Europa's floating ice shell. *Geophysical Research Letters*, *26*(7), 951–954. https://doi.org/10.1029/1999gl900125

Melosh, H., Ekholm, A., Showman, A., & Lorenz, R. (2004). The temperature of Europa's subsurface water ocean. *Icarus*, *168*(2), 498–502. https://doi.org/10.1016/j.icarus.2003.11.026

MITgcm Group. (2021). *MITgcm user manual (online documentation)*. MIT/EAPS. Retrieved from https://mitgcm.readthedocs.io/en/latest/

Moore, W. B., & Schubert, G. (2000). The tidal response of Europa. *Icarus*, *147*(1), 317–319. https://doi.org/10.1006/icar.2000.6460

Morrison, F. A. (2001). *Understanding rheology* (Vol. 1). Oxford University Press.

Ojakangas, G. W., & Stevenson, D. J. (1989). Thermal state of an ice shell on Europa. *Icarus*, *81*(2), 220–241. https://doi.org/10.1016/0019-1035(89)90052-3

Pappalardo, R., Belton, M., Breneman, H., Carr, M., Chapman, C., Collins, G., et al. (1999). Does Europa have a subsurface ocean? Evaluation of the geological evidence. *Journal of Geophysical Research*, *104*(E10), 24015–24055. https://doi.org/10.1029/1998je000628

Pappalardo, R., Vance, S., Bagenal, F., Bills, B., Blaney, D., Blankenship, D., et al. (2013). Science potential from a Europa lander. *Astrobiology*, *13*(8), 740–773. https://doi.org/10.1089/ast.2013.1003

Rambaux, N., van Hoolst, T., & Karatekin, Ö. (2011). Librational response of Europa, Ganymede, and Callisto with an ocean for a non-Keplerian orbit. *Astronomy & Astrophysics*, *527*, A118. https://doi.org/10.1051/0004-6361/201015304

Roth, L., Saur, J., Retherford, K. D., Strobel, D. F., Feldman, P. D., McGrath, M. A., & Nimmo, F. (2014). Transient water vapor at Europa's south pole. *Science*, *343*(6167), 171–174. https://doi.org/10.1126/science.1247051

Rovira-Navarro, M., Rieutord, M., Gerkema, T., Maas, L. R., van der Wal, W., & Vermeersen, B. (2019). Do tidally-generated inertial waves heat the subsurface oceans of Europa and Enceladus? *Icarus*, *321*, 126–140. https://doi.org/10.1016/j.icarus.2018.11.010

Sarid, A. R., Greenberg, R., Hoppa, G. V., Geissler, P., & Preblich, B. (2004). Crack azimuths on Europa: Time sequence in the southern leading face. *Icarus*, *168*(1), 144–157. https://doi.org/10.1016/j.icarus.2003.11.021

Shoemaker, E. M., & Wolfe, R. F. (1982). Cratering time scales for the Galilean satellites. In D. Morrison (Ed.), *Satellites of Jupiter* (pp. 277–339). University of Arizona Press.

Soderlund, K. M. (2019). Ocean dynamics of outer solar system satellites. *Geophysical Research Letters*, *46*(15), 8700–8710. https://doi.org/10.1029/2018GL081880

Soderlund, K. M., Schmidt, B. E., Wicht, J., & Blankenship, D. D. (2014). Ocean-driven heating of Europa's icy shell at low latitudes. *Nature Geoscience*, *7*(1), 16–19. https://doi.org/10.1038/ngeo2021

Sparks, W., Hand, K., McGrath, M., Bergeron, E., Cracraft, M., & Deustua, S. (2016). Probing for evidence of plumes on Europa with HST/STIS. *The Astrophysical Journal*, *829*(2), 121. https://doi.org/10.3847/0004-637x/829/2/121

Thomson, R. E., & Delaney, J. R. (2001). Evidence for a weakly stratified Europan ocean sustained by seafloor heat flux. *Journal of Geophysical Research*, *106*(E6), 12355–12365. https://doi.org/10.1029/2000je001332

Tobie, G., Choblet, G., & Sotin, C. (2003). Tidally heated convection: Constraints on Europa's ice shell thickness. *Journal of Geophysical Research*, *108*(E11), 5124. https://doi.org/10.1029/2003je002099

Tyler, R. H. (2008). Strong ocean tidal flow and heating on moons of the outer planets. *Nature*, *456*(7223), 770–772. https://doi.org/10.1038/nature07571

Vance, S., & Goodman, J. (2009). Oceanography of an ice-covered moon. In R. T. Pappalardo, W. B. McKinnon, & K. Khurana (Eds.), *Europa* (pp. 459–482). The University of Arizona Press.

Zeng, Y., & Jansen, M. F. (2021). Ocean circulation on enceladus with a high versus low salinity ocean. arXiv preprint arXiv:2101.10530.